

Dipole moment scaling for convection-driven planetary dynamos

Peter Olson ^{a,*}, Ulrich R. Christensen ^b

^a *Department of Earth and Planetary Sciences, Johns Hopkins University, Baltimore, MD, USA*

^b *Max-Planck-Institut für Sonnensystemforschung, Katlenburg-Lindau, Germany*

Received 26 January 2006; received in revised form 10 July 2006; accepted 3 August 2006

Available online 18 September 2006

Editor: S. King

Abstract

Scaling laws are derived for the time-average magnetic dipole moment in rotating convection-driven numerical dynamo models. Results from 145 dynamo models with a variety of boundary conditions and heating modes, covering a wide section of parameter space, show that the time-average dipole moment depends on the convective buoyancy flux F . Two distinct regimes are found above the critical magnetic Reynolds number for onset of dynamo action. In the first regime the external magnetic field is dipole-dominant, whereas for larger buoyancy flux or slower rotation the external field is dominated by higher multipoles and the dipole moment is reduced by a factor of 10 or more relative to the dipolar regime. For dynamos driven by basal heating, the dipole moment M increases like $M \sim F^{1/3}$ in the dipolar regime. Reversing dipolar dynamos tend to cluster near the multipolar transition, which is shown to depend on a local Rossby number parameter. The geodynamo lies close to this transition, suggesting an explanation for polarity reversals and the possibility of a weaker dipole earlier in Earth history. Internally heated dynamos generate smaller dipole moments overall and show a gradual transition from dipolar to multipolar states. Our scaling yields order of magnitude agreement with the dipole moments of Earth, Jupiter, Saturn, Uranus, Neptune, and Ganymede, and predicts a multipolar-type dynamo for Mercury.

© 2006 Elsevier B.V. All rights reserved.

Keywords: Dipole moment; Dynamo models; Planetary magnetic fields; Planetary cores; Rotating convection

1. Introduction

Planets and satellites in the solar system with active dynamos have magnetic dipole moments that span nearly eight orders of magnitude [1]. In spite of major differences in structure, composition, and history, most of these dynamos are thought to be maintained by similar mechanisms: thermal and compositional convection in electrically conducting fluids in the planet interiors [2]. In

addition to active dynamos in Earth, Mercury, Jupiter, Saturn, Neptune, Uranus and Ganymede, extinct convective dynamos have been proposed for Mars [3] and the Moon [4]. In contrast Venus has an iron core that may be convecting, but has no dynamo [37].

The search for a unified theory linking dipole moments to the structure and dynamics of planetary interiors has led to a number of proposed magnetic scaling laws [5–9]. Initially these were derived using dimensional analysis and simplified physical arguments, usually in the form of power-law relationships between the dipole moment and basic physical properties such as radius, rotation rate, angular momentum, density, and

* Corresponding author. Tel.: +1 410 516 7707; fax: +1 410 516 7933.

E-mail address: olson@jhu.edu (P. Olson).

Table 1
Earth's core physical properties

Parameter	Notation	Units	Value
Dipole moment	M	A m ²	7.8×10^{22}
Core radius	r_o	m	3.48×10^6
Inner core radius	r_i	m	1.22×10^6
Outer core thickness	d	m	2.26×10^6
Rotation rate	Ω	rad s ⁻¹	7.29×10^{-5}
Density	ρ	kg m ⁻³	11×10^3
Electrical conductivity	σ	A ² kg ⁻¹ m ⁻³ s ³	6×10^5
Magnetic diffusivity	λ	m ² s ⁻¹	1.3
Buoyancy flux	F	m ² s ⁻³	2×10^{-13}

electrical conductivity. More recently, they have been generalized to include dependence on the dynamo energy source, convection in this case [23]. Such heuristic scaling laws allow for easy comparison between diverse planetary magnetic fields, but because their physical content is so limited, they have been only partly successful in rationalizing the known planetary dipole moments and predicting the values of newly discovered ones [7,10,38].

Numerical dynamos are now used to model planetary magnetism, with considerable success. Numerical dynamos driven by Boussinesq convection in thick, rotating fluid shells commonly produce magnetic fields similar to the geomagnetic field, with a strong axial dipole component, secular variation, and occasional polarity reversals [11–13]. Convection-driven dynamo models in thin shell geometries sometimes produce inclined dipolar or multipolar fields, suggestive of the magnetic fields of Neptune and Uranus [14,15] and possibly Mercury [53,54]. Dynamo models with inner cores smaller than the present Earth predict different magnetic field intensity at early stages of inner core growth [16].

However, problems remain in applying numerical dynamo model results directly to the planets. Some of these problems stem from our limited knowledge of planetary interiors, but others arise because the dynamo models are far removed in parameter space from the planets. Specifically, numerical dynamos rotate too slowly, are less turbulent, and have far too large viscosity (relative to electrical conductivity) compared to their planetary counterparts [17]. In terms of the dimensionless parameters that control convective dynamos, this combination of factors means that the Rayleigh number is too small, and the Ekman and magnetic Prandtl numbers are too large in the dynamo models [18]. The prospect of direct numerical simulation with realistic values of these parameters is remote, because of the enormous temporal and spatial resolution such calculations would require [19].

In this paper, scaling relationships for the dipole moment are derived from the results of numerical dynamos within the part of parameter space now accessible to computation. These relationships are then extrapolated to planetary interior conditions and compared with observed (and inferred) planetary dipole moments. Several properties of numerical dynamo models have already been analyzed this way, including the zonal fluid velocity [20,21] and Ohmic dissipation [22]. Recently, Christensen and Aubert [32] (hereafter abbreviated CA) have proposed asymptotic scaling relationships for the rms internal magnetic field strength, heat flow, and convective velocity, based on a large set of numerical dynamos. In this paper we make use of the CA scaling parameters, but we focus on the dipole moment, the most fundamental observable dynamo property. Unlike some other dynamo properties, the dipole moment does not follow an asymptotic power-law scaling.

2. Dynamo scaling parameters

In terms of standard dynamo model properties, the time average dipole moment M is defined as

$$M = \frac{4\pi r_o^3}{\sqrt{2}\mu_0} B_{\text{dip}} \quad (1)$$

Here $\mu_0 = 4\pi \times 10^{-7}$ H/m is magnetic permeability, r_o is the dynamo (outer core) radius and B_{dip} is the time average rms dipole field intensity at r_o . The time average dipole moment is a function of the input control parameters that specify a particular dynamo model. One set of control parameters that has been widely used for thermal convection dynamos [24] consists of the Prandtl number

$$Pr = \frac{\nu}{\kappa} \quad (2)$$

where ν is kinematic viscosity and κ is thermal diffusivity of the fluid, the magnetic Prandtl number

$$Pm = \frac{\nu}{\lambda} \quad (3)$$

where $\lambda = 1/\mu_0\sigma$ is magnetic diffusivity (σ is electrical conductivity), the Ekman number

$$E = \frac{\nu}{\Omega d^2} \quad (4)$$

where Ω is angular velocity of rotation and d is the fluid thickness, and a Rayleigh number

$$Ra = \frac{\alpha g q d^4}{\kappa \nu} \quad (5)$$

Table 2
Planetary core physical properties relative to earth's core

Planet	Ω	r_o	ρ	σ	M	F	d	Refs.
Venus	0.004	1.0	1.0	1.0	0.0	0.8	1.0	[39]
Mercury	0.017	0.5	0.9	1.0	0.0004	0.5	0.2	[40]
Earth	1.0	1.0	1.0	1.0	1.0	1.0	1.0	[41]
Mars ^a	1.0	0.5	0.9	1.0	0.15	2.0	0.5	[42]
Jupiter	2.42	16.0	0.16	0.1	18,000.0	100	18.0	[43–45]
Saturn	2.25	8.5	0.16	0.1	580.0	50	7.0	[46,47]
Uranus	1.39	4.9	0.18	0.03	50.0	20	5.0	[48]
Neptune	1.49	4.5	0.18	0.03	24.0	20	5.0	[49]
Moon ^a	0.07	0.12	0.9	1.0	0.001	0.3	0.12	[50]
Ganymede	1.37	0.2	0.7	1.0	0.002	0.3	0.2	[51]

^a Extinct dynamo.

where α is thermal expansivity, g is gravity on the outer boundary, q is the average superadiabatic heat flux on the outer boundary, and k is thermal conductivity. In addition, a geometrical parameter is needed for planets with a solid inner core. For these we use the radius ratio, defined as

$$r^* = \frac{r_o}{r_i} \quad (6)$$

where r_i is the inner core radius, so that $d=r_o-r_i$. Other model parameters would be needed to fully characterize compressibility, boundary heterogeneity, and inner core rotation, but in this study we consider only the above five. Units of the physical quantities in these parameters are given in Table 1, along with Earth's core values. The relative values of these parameters assumed for the other planets and satellites are given in Table 2.

Although (4) and (5) are often used as input for dynamo modelling, they are not the most suitable choices for scaling convection-driven dynamo behavior. In place of these, we use the magnetic Ekman number

$$E_\lambda = Pm^{-1}E = \frac{\lambda}{\Omega d^2} \quad (7)$$

and a buoyancy flux-based Rayleigh number Ra_Q defined by CA [32] as

$$Ra_Q = \frac{r^*F}{d^2\Omega^3} \quad (8)$$

where F is the average convective buoyancy flux. The Rayleigh number Ra_Q is advantageous in this context because it is directly proportional to the power input by buoyancy forces. The buoyancy flux in thermal convection can be expressed in terms of the convective heat flux q' as

$$F = \frac{\alpha g q'}{\rho C_p} \quad (9)$$

where C_p is specific heat and ρ is density. For base-heated convection, the conventional Rayleigh number (5) and the buoyancy flux-based Rayleigh number (8) are related by

$$Ra_Q = \frac{r^*E^3(Nu-1)}{Pr^2Nu} Ra \quad (10)$$

where

$$Nu = \frac{r^*qd}{k\Delta T} \quad (11)$$

is the time-average Nusselt number on the outer boundary, written in terms of the superadiabatic temperature difference across the spherical shell ΔT .

The conventional parameter for scaling the internal magnetic field in planetary dynamos is the Elsasser number, which has the following definition for the dipole field:

$$\Lambda_{\text{dip}} = \frac{\sigma B_{\text{dip}}^2}{\rho\Omega} \quad (12)$$

However, CA [32] argued that a better choice for scaling magnetic fields in convective dynamo models is the Lorentz number. The dipole field Lorentz number is here defined as

$$Lo_{\text{dip}} = \sqrt{E_\lambda \Lambda_{\text{dip}}} = \frac{B_{\text{dip}}}{\sqrt{\rho\mu_0}\Omega d} = \frac{\sqrt{2\mu_0/\rho}}{4\pi r_o^3 \Omega d} M \quad (13)$$

We are also interested in relating scaling laws for dipole moment to scaling laws for the convective fluid velocity. The usual scaling for dynamo fluid velocity u is the magnetic Reynolds number $Rm=ud/\lambda$, however, CA [32] have shown that a Rossby number scaling is more compatible with (8). For the time average rms fluid

velocity, we use the following definition of the global (i.e., large scale) Rossby number:

$$Ro = E_j Rm = \frac{u}{\Omega d} \quad (14)$$

In addition, it is useful to define a local (i.e., small scale) Rossby number, based on a characteristic length scale of the flow, as in CA [32]:

$$Ro_l = \frac{l_u}{\pi} Ro \quad (15)$$

in which

$$l_u = \sum_{l=0}^{l_{\max}} l \frac{\langle \mathbf{u}_l \cdot \mathbf{u}_l \rangle}{\langle \mathbf{u} \cdot \mathbf{u} \rangle} \quad (16)$$

where \mathbf{u}_l is the spherical harmonic degree l component of the vector velocity \mathbf{u} and the angle brackets denote rms.

3. Data selection

Numerical data from different numerical dynamo calculations were extracted from a variety independently conducted, systematic modeling studies [12,18,26–32]. To test the robustness of the scaling, data was included from 125 published dynamos with both rigid and stress-free velocity boundary conditions, as well as fixed temperature and fixed heat flux thermal boundary conditions. In addition, we have included 20 unpublished dynamos driven by uniform volumetric (internal) heat generation, which simulate the effects of radioactive decay and secular cooling. All models used in this study assume Boussinesq conditions and all employ constant diffusion coefficients (i.e., no hyperdiffusivity). Most assume a geometry close to Earth's core, some include inner core rotation, and others include core–mantle boundary heat flow heterogeneity. Because most numerical dynamo models exhibit dipole moment fluctuations and some include dipole polarity reversals, we have used time-average dipole moments, fluid velocities, and heat flows throughout this study, except for the data from [12] which were based on snap-shot values. Included in the data are seven subcritical and failed dynamos, which were added to help define the regime transitions.

Since the various modeling studies used different schemes of nondimensionalization, the first step was to tabulate all the data in terms of the conventional parameters Pr , Pm , E , Ra , Rm , Nu , and either B_{rms} or M . Time averages of these quantities were typically computed over several dipole diffusion times, and then converted to E_λ , Ra_Q , Lo_{dip} , and Ro , as defined in (7), (8), (13), and (14),

respectively. For base-heated dynamos, the total (i.e., surface-integrated) buoyancy flux is independent of radius, and for these cases there is no ambiguity in the definition of Nu , F , and Ra_Q . For internally heated dynamos however, the Nusselt number and the total buoyancy flux are radius-dependent. For these cases we used the volume-average Nusselt number in calculating Nu and Ra_Q . As illustrated in Fig. 1 the model data space covers the ranges $3 \times 10^{-6} \leq E \leq 10^{-2}$, and $10^4 \leq Ra \leq 1.5 \times 10^{10}$, and also $0.06 \leq Pm \leq 24$, $0.1 \leq Pr \leq 20$. In all cases we use $r^* = 2.85$, appropriate for the Earth's core. Different studies used different amounts of numerical resolution. Typical spherical harmonic truncations were $l_{\max} = 64$, 106, and 200 for $E = 3 \times 10^{-4}$, 3×10^{-5} , and 3×10^{-6} , respectively, although [12] and [18] used $l_{\max} = 256$ and 384, respectively.

4. Velocity scaling results

Scaling laws that are independent of, or only weakly dependent on, the small diffusion coefficients are especially useful because the values of the diffusion coefficients in planetary cores are either highly uncertain or cannot be matched in numerical models. This is particularly true for the kinematic viscosity. Recently, several diffusivity-free scaling laws for velocity have been found by assuming the Rossby number Ro depends on the Rayleigh number Ra_Q , and is independent of E_λ , Pr , and Pm . For example, a scaling law has been proposed for the time-average zonal part of the fluid velocity in convective dynamos [20,21] of the form

$$Ro_{\text{zonal}} \approx (2Ra_Q)^{1/2} \quad (17)$$

and CA [32] found $Ro = 0.85 Ra_Q^{0.41}$ for the rms velocity in convective dynamos with rigid, isothermal boundaries.

The upper panel in Fig. 2 shows the variation of Ro with Ra_Q in the more diverse set of dynamos used in this study. Our velocity data define two nearly parallel trends, one for all of the base-heated cases, the other for the internally heated cases. The base-heated cases are well-approximated by

$$Ro = \beta Ra_Q^{2/5} \quad (18)$$

with $\beta \approx 0.85$, very close to the results of CA [32]. For the internally heated dynamos, number of cases and the parameter range is more limited, although the same 2/5-power-law with $\beta \approx 0.43$ provides a reasonably good fit. In terms of dimensional variables, for an Earth-like geometry with $r^* = 2.85$ and $\beta = 0.85$, (18) is equivalent to

$$u \approx 1.3(d/\Omega)^{1/5} F^{2/5} \quad (19)$$

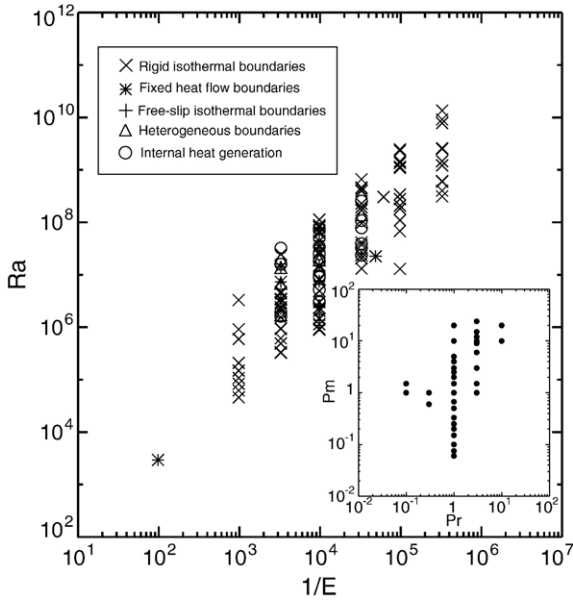


Fig. 1. Parameter range of numerical dynamo models used for dipole moment and convective velocity scaling. Ra and E are heat flow-based Rayleigh number and Ekman number, respectively, with symbols indicating the various model boundary and heating conditions. Insert shows the range of Prandtl numbers Pr and Pm , respectively.

A similar formula applies to internally heated dynamos, but with a coefficient of about 0.66.

Eq. (19) indicates that the rms fluid velocities in dynamos driven either by basal or internal heating can be expressed in terms of buoyancy flux, fluid layer depth, and the rotation period (inverse rotation rate) without explicit dependence on the diffusion coefficients (including the kinematic viscosity and the magnetic and thermal diffusivities). It is somewhat unexpected that this power-law fits such a diverse set of dynamos, because it is well known that the choice of boundary conditions and diffusivities have big effects on dynamo model velocities. Evidently most of these effects are subsumed in (18) by defining the Rayleigh number in terms of the convective buoyancy flux. CA [32] found a marginally better fit than (18) by introducing a weak dependence of the of Ro on the magnetic Prandtl numbers. That procedure applied to this data failed to yield a significantly better fit than shown in Fig. 2.

We have also determined the dependence of the local Rossby number Ro_l on the fundamental control parameters, by fitting (16) to power-law products of (2), (3), (7), and (8). In contrast to the large-scale Rossby number, which depends to first order only on Ra_Q , we find that all four basic parameters have an influence on Ro_l . In Fig. 3

we show that a reasonably good fit is obtained by the following expression:

$$Ro_l = 0.58 Ra_Q^{1/2} E^{-1/3} Pr^{1/5} Pm^{-1/5}. \quad (20)$$

In terms of dimensional variables and parameters, (20) is approximately

$$Ro_l \approx \frac{(\lambda/\kappa)^{1/5} F^{1/2}}{(vd)^{1/3} \Omega^{7/6}} \quad (21)$$

so that Ro_l increases with buoyancy flux, decreases with rotation rate, and is weakly dependent on all three diffusion coefficients.

5. Dipole moment scaling results

Unlike fluid velocity, we found no asymptotically-valid power law scaling for the time-average dipole moments. Instead the dipole moment shows separate regimes of behavior. Fig. 4 illustrates schematically the relationship between the various regimes in the dipole moment — Rayleigh number plane, for fixed values of the other parameters. Dynamo action first occurs beyond the onset of convection at a Rayleigh number value that corresponds to a critical magnetic Reynolds number

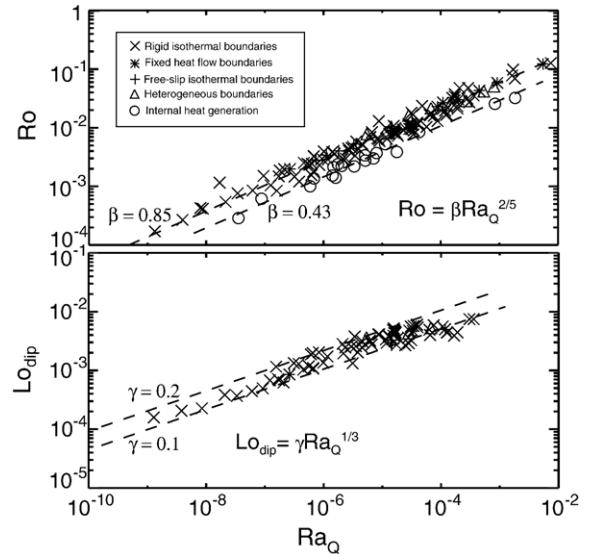


Fig. 2. Fluid velocity and dipole moment versus buoyancy flux Rayleigh number from numerical dynamos. Top: Rossby number for fluid velocity. Dashed lines show fits to 2/5-power-law for base-heated and internally heated cases, respectively. Bottom: Lorentz number for dipole moment from base-heated, dipole-dominant dynamos with Nusselt numbers $Nu > 1.9$. Dashed lines show fits to 1/3-power-law envelope.

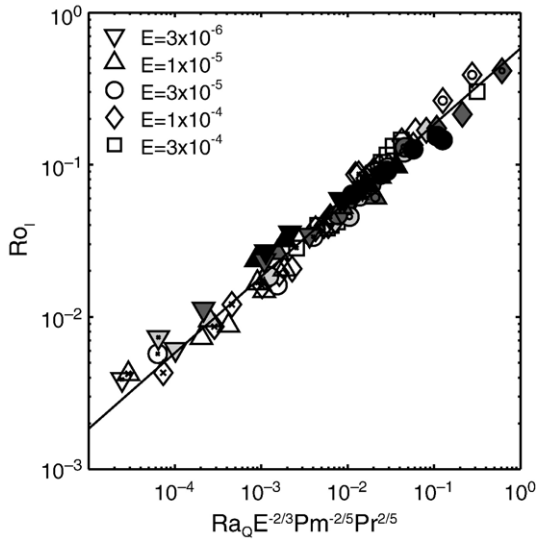


Fig. 3. Local Rossby number versus a power-law combination of the control parameters for the model data used by CA [32]. The shape of the symbol indicates the value of the Ekman number and the shading the value of Pm , where darker means lower value. Exponents of the four control parameters were found by least squares fit constrained to small integer fractions. Slope of best-fit line is 0.5. The average relative misfit to Eq. (20) is 17%.

Rm_{crit} . This behavior is shown in Fig. 5, where the dipole moment Lorentz number Lo_{dip} increases rapidly from zero to a finite value around $Rm_{crit} \approx 40$, irrespective of the other parameters. Fig. 5 also shows that beyond Rm_{crit} there is no simple relationship between Lo_{dip} and Rm , indicating that a different parameter (or set of parameters) is needed to scale finite dipole moments.

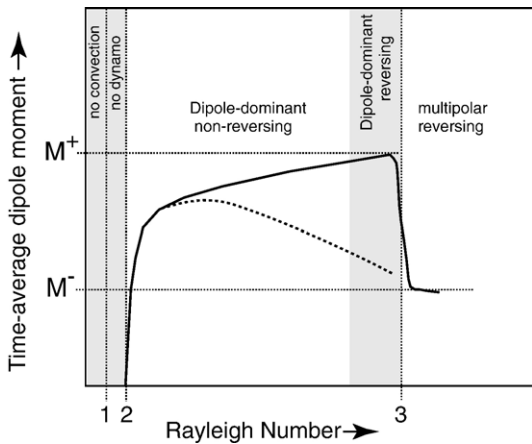


Fig. 4. Schematic illustration of dynamo regimes, showing variation of time-average dipole moment versus Rayleigh number with other parameters fixed. Solid line corresponds to base-heated dynamos, dashed line to internally heated dynamos.

Referring to Fig. 4, as the Rayleigh number is systematically increased beyond the onset of dynamo action, and after its initial rapid rise, the dipole moment increases slowly with Rayleigh number up to a peak value, then drops to much smaller values as the Rayleigh number is increased further. In the first regime, labeled “dipolar” in Fig. 4, the magnetic field on the outer boundary is dominated by a strong dipole component, with weaker higher multipole fields. In the next regime, labeled “multipolar” in Fig. 4, the dipole is weaker than some of the higher multipole components on the outer boundary. The Rayleigh number interval which marks the transition from dipolar to multipolar states depends on the values of the other control parameters, as does the magnitude of the dipole moment drop across the transition. The transition may be abrupt in some cases and gradual in others, as depicted by the solid and dashed lines in Fig. 4. Dynamo modeling studies have shown that dipole reversals are frequent in the multipolar regime, and in the dipolar regime they often occur near this transition [27,28].

The lower panel in Fig. 2 shows the variation in dipole moment in the dipole-dominant regime, in terms of Lo_{dip} versus Ra_Q . This plot includes only dynamo models with (i) dipole-dominant fields on the outer boundary; (ii) basal heating, and (iii) $Nu > 1.9$, cases which were judged to have reached a fully-developed convective state. For dynamos satisfying these three restrictions, we find that the dipole Lorentz number increases monotonically with Rayleigh number, although there is some scatter. The

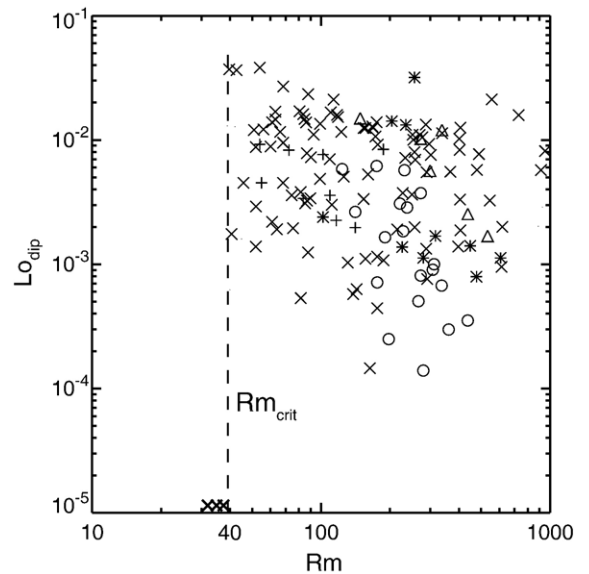


Fig. 5. Dimensionless dipole moment Lo_{dip} versus magnetic Reynolds number Rm showing onset of dynamo action near $Rm_{crit} \approx 40$. Symbols as in Fig. 2. Clipped data denote failed dynamos.

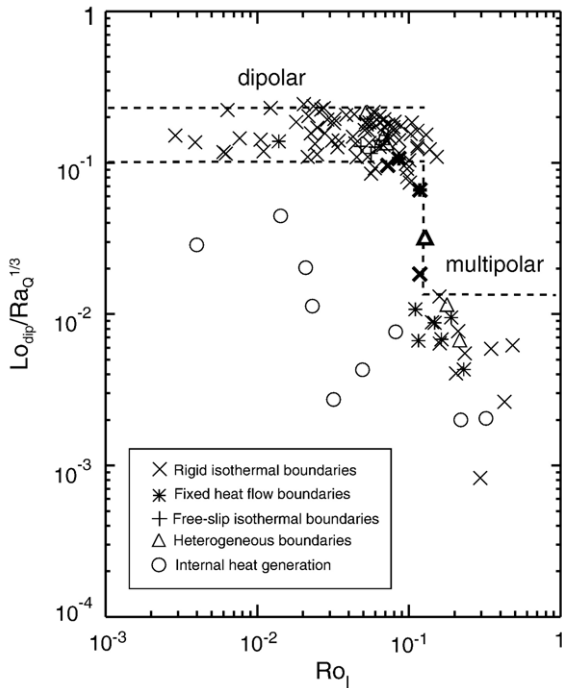


Fig. 6. Dimensionless dipole moment (normalized by Rayleigh number) versus local Rossby number for all dynamos with Nusselt number greater than 1.9, showing the transition from dipolar to multipolar regimes. Reversing dipole-dominant cases are plotted with bold symbols and cluster near the transition. Note that internally-heated cases (circles) follow a different trend than the base-heated cases.

dashed lines in the lower panel Fig. 2 define an approximate envelope for the data and correspond to

$$Lo_{dip} = \gamma Ra_Q^{1/3} \quad (22)$$

with the coefficients γ equal to 0.1 and 0.2 for the upper and lower curves, respectively. In terms of dimensional variables, (22) is equivalent to

$$M \approx 4\pi r_o^3 \gamma (\rho/\mu_o)^{1/2} (Fd)^{1/3} \quad (23)$$

where we have again used an Earth-like $r^*=2.85$. According to (23) the dipole moment increases with convective buoyancy flux as $M \sim F^{1/3}$ in this regime and shows no explicit dependence on planetary rotation rate Ω .

There is an indication in Fig. 2 of a systematic deviation from (22), particularly at large Ra_Q , where the Lo_{dip} -values seem to approach saturation. We attempted to resolve possible additional dependencies by fitting the dipole moments in Fig. 2 to parameter groups involving products of fractional powers of the Prandtl numbers, for example $Lo_{dip} Pr^\epsilon Pm^\delta$. This additional freedom did not substantially reduce the scatter in Fig. 2, and since it introduces dependence on the uncertain diffusivities (including

viscosity) we conclude that it does not meaningfully improve the dipole moment scaling in this regime. It is very likely that some of the scatter in Fig. 2 is due to the variety of boundary conditions represented in the data, different symmetry constraints used in some models, and errors in estimating true time-averages from finite-duration calculations, in addition to the possible weak Prandtl number dependence. We note that CA obtained results comparable to (22) and (23) for the rms internal magnetic field strength, with somewhat different coefficients and without evidence of saturation. They also found marginally better fits by allowing weak dependance on the diffusivities and the relative amount of Ohmic heat production.

As Ra_Q is increased, the dipole moment deviates from (22) and (23), and the dynamos transition to the multipolar regime. Fig. 6 shows this transition, expressed as the variation of $Lo_{dip}/Ra_Q^{1/3}$ (the parameter combination in the dipolar regime) versus the local Rossby number Ro_l . Fig. 6 includes all the successful dynamos with $Nu > 1.9$, including those driven by volumetric heat sources. For the base-heated dynamos, the transition from dipole-dominant to multipolar dynamos occurs in a narrow interval around $Ro_l \approx 0.12$. Across this transition the dipole moment falls by nearly a factor of 20. Further increase in Ra_Q results in a partial rebound of the dipole moment in some cases, but in other cases it results in additional decrease. The internally heated dynamos show a different behavior. Although there are fewer internally heated cases in our study and they cover a more limited slice of parameter space, it is clear that their dipole moments are systematically weaker than comparable base-heated cases, the transition from dipolar to multipolar states is more gradual, shows more scatter, and it begins at smaller Ro_l -values.

Several properties connected with the dipolar–multipolar transition in Fig. 6 might be important for the geomagnetic field and other planetary magnetic fields. First, dynamo models with reversing, dipole-dominant fields tend to cluster near the transition. This group is indicated with bold symbols in Fig. 6 and includes models with widely different control parameters and distinct modes of polarity reversal (i.e., dynamos with periodic and irregular reversals). Their overlap in Fig. 6 suggests that the likelihood for polarity reversal in an otherwise stable dipole-dominant dynamo may be controlled by its proximity to the multipolar transition. The localization of reversing dipolar dynamos in this part of parameter space is implicit in an early study by Gilman [55], who attributed the effect to the presence of strong toroidal flows, rather than fluid inertia. Second, the base-heated dynamos have fairly well-defined characteristic dipole moment values on either side of the transition; in Fig. 4 these are denoted by M^+ and M^- , respectively. On the

Table 3
Planetary core convection parameters

Planet	E_λ	Ra_Q	Ro	Ro_l	Lo_{dip}	M (calc)	M (obs)
Mercury ^a	5×10^{-6}	3×10^{-7}	2×10^{-3}	8	1.4×10^{-5}	0.1	0.031
Venus ^a	9×10^{-7}	4×10^{-6}	5×10^{-3}	50	≈ 0	≈ 0	≈ 0
Earth	3.5×10^{-9}	3×10^{-13}	8×10^{-6}	0.09	1.4×10^{-5}	74	78
Moon ^b	3×10^{-6}	1×10^{-8}	5×10^{-4}	2	9×10^{-4}	0.04	≈ 0.08
Mars ^b	1×10^{-8}	2×10^{-12}	2×10^{-5}	0.1	2.4×10^{-5}	9	≈ 8
Jupiter	4.5×10^{-12}	8×10^{-17}	3×10^{-7}	0.01	1.1×10^{-6}	1.6×10^6	1.4×10^6
Ganymede	6×10^{-8}	8×10^{-13}	1×10^{-5}	0.05	1.5×10^{-5}	0.19	0.16
Saturn	3×10^{-11}	2×10^{-16}	4×10^{-7}	0.01	6.6×10^{-7}	11×10^4	4.5×10^4
Uranus	1×10^{-10}	8×10^{-17}	3×10^{-7}	.005	3.5×10^{-7}	17×10^3	3.9×10^3
Neptune	9×10^{-11}	8×10^{-17}	3×10^{-7}	.005	2×10^{-7}	14×10^3	1.9×10^3

M in units of 10^{21} A m².

^a Multi-polar field scaling.

^b Extinct dynamo.

dipolar side, (22) and (20) with $Ro_l=0.12$ give a peak dipole moment of approximately

$$M^+ \approx 3\gamma\Omega r_0^3 d (\rho/\mu_0)^{1/2} (\kappa/\lambda)^{2/15} E^{2/9} \quad (24)$$

with $M^- \approx 0.05M^+$ on the multipolar side. In contrast, the internally heated cases have smaller moments in the dipolar regime and do not show characteristic values. A third implication of Fig. 6 concerns changes in magnetic field structure with time that would accompany secular changes in Ro_l and Ra_Q . We discuss some implications of these effects for the Earth and other planets in the following sections.

6. Comparison with planetary dynamos

We have applied the scaling laws derived in the previous section to planetary dynamos using the physical parameter data in Tables 1 and 2. Some of the physical parameters, such as λ and M , are reasonably well constrained for all these planets and satellites, whereas others such as d and F are known only for a few. Estimates of the buoyancy flux F in the Earth's core come from energy constraints and thermal history considerations [33–35], and estimates of F in Jupiter and Saturn come from their excess luminosity [36]. The buoyancy flux in the other planets is highly uncertain, and in some cases even its sign is controversial. Here we have chosen to scale the buoyancy flux of the terrestrial planets with active dynamos relative to the Earth, in proportion to their respective core surface areas (for the ancient Lunar and Martian dynamos we assume twice this flux). Likewise we scale the buoyancy flux of the gas planets relative to Jupiter in proportion to their respective conducting fluid surface areas. These rules are used in the absence of

stronger constraints, and may fail to account for important differences in the present state of planetary interiors brought about by differences in planetary evolution (i.e., thermal history) and other factors not considered here. For example, we assume a positive buoyancy flux in all planets in Table 2, contrary to models that postulate stable stratification for some planets, Venus in particular [37]. For completeness we also include in Table 2 parameter estimates for the proposed ancient dynamos in Mars and the Moon, and the hypothesized dynamo in Ganymede [51] with Earth-like conductivities assumed.

In spite of the large uncertainties in some critical parameters, we find similarities with the dipole moments of several planets. Table 3 summarizes our planetary scaling results and compares the predicted with the observed dipole moments of the presently active planetary dynamos and the dipole moments inferred for the extinct ones. Fig. 7 shows planetary dipole moments scaled with the same dimensionless parameters used for the numerical dynamos in Fig. 6. The darkly shaded region in Fig. 7 corresponds to (22) with upper and lower bounds of $\gamma=0.1$ and 0.25 , respectively. The dipole moments of Jupiter, Earth, Saturn, and Ganymede lie within or near the dipole-dominant region for base-heated convection, with Saturn lying slightly below and Jupiter slightly above the average of this group. The Earth plots close to the multipolar transition, where the reversing dipolar dynamos are concentrated.

The dipole moments of Uranus and Neptune are relatively weaker than the main group, and plot below the dipolar regime for base-heated dynamos, within the range of internally heated dynamos. In contrast to the other magnetic planets in the main group, the external magnetic fields of Neptune and Uranus are not strongly dominated by the axial dipole component [48,49]. Possibly the convection in these planets is not fully developed (i.e.,

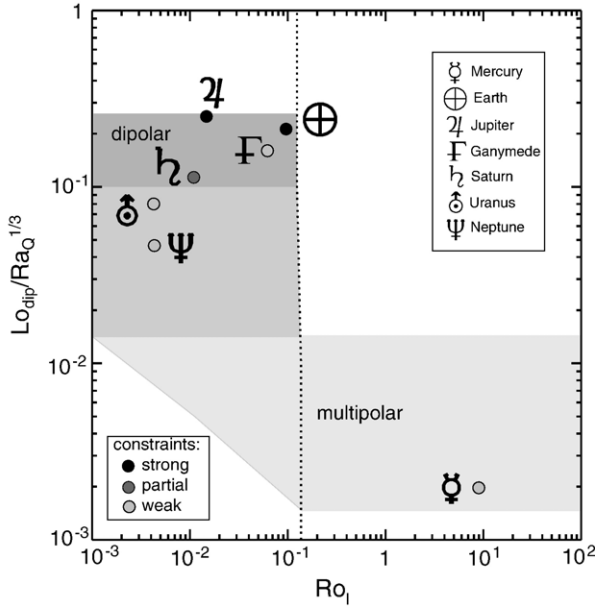


Fig. 7. Dimensionless planetary dipole moment (normalized by Rayleigh number) versus local Rossby number. The transition from strongly dipolar (dark shading) to multipolar (light shading) regimes from Fig. 6 is shown for comparison. The planets are shaded in proportion to the strength of the constraints on the control parameters Ra_Q and Ro_l .

characterized by a small Nusselt number) or perhaps there are geometrical effects such as a thin convecting layer [14], whose effects are not properly represented in our scaling. An alternative interpretation suggested by Fig. 7 is that these dynamos are driven primarily by secular cooling, which may act like volumetric heat sources, producing a relatively weak dipole moment. This same argument does not apply so well to Jupiter, which has a strong dipole and, yet, is thought to be driven largely by secular cooling [2].

The location of these six planets in Fig. 7, and the order-of-magnitude agreement between their observed and predicted moments in Table 3, suggests they are fundamentally within the same convective dynamo family, with some variations due to differences in core geometry, heating modes, and other factors. The situation appears different for Mercury. As shown in Fig. 7, Mercury lies in the multipolar region, far from the main dipolar sequence. This is consistent with recent model results [53,54] that find multipolar fields in dynamo models with the thin-shell core geometry often assumed for Mercury. According to our scaling, the combination of thin-shell geometry and the slow rotation rate implies a large local Rossby number $Ro_l \approx 8$ in Mercury, and hence a multipolar field. Venus occupies an even more extreme position in this scheme, with a predicted Ro_l -value of nearly 50.

Fig. 8 shows the planetary dynamos in the Rayleigh number–magnetic Ekman number plane, with the

estimated locations of the extinct Lunar and Martian dynamos included for comparison purposes. In this figure we use another buoyancy flux-based Rayleigh number

$$Ra_F = \frac{Fd^2}{\lambda^2 \Omega} = \frac{Ra_Q}{r^* E_\lambda^2} \quad (25)$$

which allows the location of the dipolar–multipolar transition for base-heated convection to be superimposed on contours of the magnetic Reynolds number of the convection calculated from (18) and (14). Here we have assumed nominal values $Pm=10^{-5}$ and $Pr=1$ in determining Ro_l . Since the critical convective velocity for dynamo onset corresponds to about $Rm \approx 40$, Fig. 8 indicates that all the planets have (or had, in the case of the Moon and Mars) internal convective velocities above the critical Rm for dynamo action. Ganymede and the ancient Lunar dynamo have rather small magnetic Reynolds numbers, of the order $Rm \approx 200$, according to this scaling, whereas all the others are far beyond critical. In the case of the Earth, our scaling predicts a convective $Rm \approx 2300$. This is several times larger than Rm estimated for large-scale core motions from the geomagnetic secular variation, but comparable to the Rm estimated directly from the characteristic time constants of secular variation as a function of spherical harmonic degree [22].

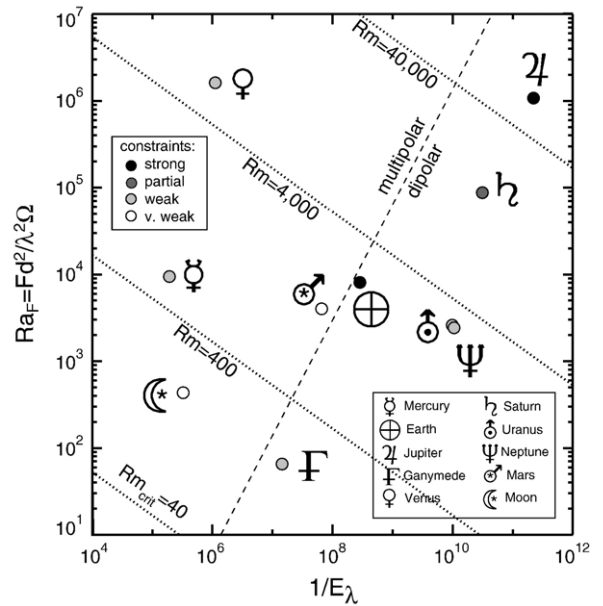


Fig. 8. Parameter range of planet cores assuming convective scaling. Ra_F and E_λ are modified buoyancy flux-based Rayleigh number and magnetic Ekman number defined by (25) and (7), respectively. Dashed line indicates approximate dipolar–multipolar transition for base-heated dynamos. Broken contours indicate constant values of magnetic Reynolds number Rm . Asterisks denote extinct dynamos.

7. Discussion

The transition from dipolar to multipolar states has implications for some planetary dynamos. This transition is reported in several previous studies of base-heated dynamos [25–27] and has been attributed to emergence of inertia as a ranking term in the force balance [32,52]. Support for this interpretation can be found in the change in flow structures across the transition. In the dipolar regime, particularly at low Ro_I -values, the convection is dominated by columns of axial vorticity that are continuous (or nearly continuous) across the fluid shell. In the multipolar regime these columnar structures become distorted and break into irregular vortex filaments [26]. The standard view is that inertia is unimportant in most planetary dynamos, in comparison with the Coriolis acceleration [23]. This view is justifiable for the larger scales of motion, for example, the motion in Earth's core imaged by the geomagnetic secular variation. But at the scale of the convection, the results in Fig. 7 indicate that inertia plays some role, especially in the Earth and in Mercury. For example, we find $Ro_I \approx 0.09$ for the Earth's core, implying a convective length scale of a few kilometers.

Reversing dipolar dynamos tend to cluster near the transition, suggesting a connection with geomagnetic polarity reversals. Suppose that the time-average state of the geodynamo is close to the transition (but within the dipolar regime, as in Fig. 7) so that fluctuations about its mean state sometimes result in excursions into the multipolar regime. In dynamical terms, these fluctuations might arise during bursts of outer core convection, producing excess buoyancy flux and temporarily larger Ro_I -values. After the excess buoyancy has been released and dissipated the geodynamo would return to its usual dipolar state, possibly with reversed polarity. In this scenario, periods with frequent reversals and excursions would correspond to energetic (high Ro_I , high variability) dynamo states, and superchrons to quiet (low Ro_I , low variability) dynamo states.

The results in Fig. 7 may also be relevant to the long-term evolution of the geodynamo. Thermal history models indicate that the buoyancy flux F has changed with time, due to secular cooling and inner core growth [34,35]. Similarly, tidal friction predicts that the rotation rate Ω has decreased with time. Since both of these changes affect Ra_Q and Ro_I , it is possible that the geodynamo occupied different positions in Fig. 7 earlier in Earth history, in which case the dipole moment may have been significantly weaker than today. We note that the peak (sustained) dipole moment for the Earth predicted by (24) is approximately $M^+ \approx 10 \times 10^{22} \text{ A m}^2$.

Lastly we consider the practical problem of finding numerical dynamo models with large Ekman and magnetic Prandtl numbers that correctly scale to planetary magnetic fields. For example, a typical dynamo model with $E=10^{-4}$, $r^*=2.85$, and $Pr=Pm=1$ has an “Earth-like” Ro_I -value for $Ra_Q \approx 6.5 \times 10^{-5}$, or alternatively $Ra \approx 2.5 \times 10^7$. The Rossby and Lorentz numbers predicted by our scaling for this model are $Ro \approx 1.8 \times 10^{-2}$ and $Lo_{\text{dip}} \approx 8 \times 10^{-3}$. The fact that these exceed the estimated Earth values by several orders of magnitude (see Table 3) illustrates the importance of accurate scaling laws for planetary dynamo modeling. Additional calculations are therefore needed, to determine the sensitivity to variations in fluid shell depth, smaller Ekman and magnetic Prandtl numbers, alternative forms of boundary heterogeneity, fluid compressibility, stable stratification, turbulence parameterizations, and other effects that are likely to be important in planets but have not been considered here.

Acknowledgments

This work has been supported by NASA grant NAG5-11220, by the NSF Geophysics Program, and by the DFG priority program Geomagnetic Secular Variations.

References

- [1] I. De Pater, J.J. Lissauer, Planetary Sciences, Cambridge University Press, 2001 528 pp.
- [2] D.J. Stevenson, Planetary magnetic fields, Earth Planet. Sci. Lett. 208 (2003) 1–11.
- [3] B.P. Weiss, V. Hoyatollah, F.J. Beudenbachere, J.L. Kirschvink, S.T. Steward, D.L. Shuster, Records of an ancient Martian magnetic field in ALH84001, Earth Planet. Sci. Lett. 201 (2002) 449–463.
- [4] D.R. Stegman, M. Jellinek, S.A. Zatman, et al., Lunar core dynamo driven by thermochemical mantle convection, Nature 421 (2003) 143–145.
- [5] P.M.S. Blackett, The magnetic field of massive rotating bodies, Nature 159 (1947) 658–666.
- [6] F.H. Busse, Generation of planetary magnetism by convection, Phys. Earth Planet. Inter. 12 (1976) 350–358.
- [7] D.J. Stevenson, Planetary magnetic fields, Rep. Prog. Phys. 46 (1983) 555–620.
- [8] S.A. Curtis, N.F. Ness, Magnetostrophic balance in planetary dynamos: predictions for Neptune's magnetosphere, J. Geophys. Res. 91 (1986) 11,003–11,008.
- [9] Y. Sano, The magnetic fields of the planets: a new scaling law of the dipole moments of the planetary magnetism, J. Geomagn. Geoelectr. 45 (1993) 65–77.
- [10] J.C. Cain, P. Beaumont, W. Holter, Z. Wang, H. Nevanlinna, The magnetic Bode fallacy, J. Geophys. Res. 100 (1995) 9439–9454.
- [11] G.A. Glatzmaier, R.S. Coe, L. Hongre, P.H. Roberts, The role of the mantle in controlling the frequency of geomagnetic reversals, Nature 401 (1999) 885–890.

- [12] F. Takahashi, M. Matsushima, Y. Honkura, Simulations of a quasi-Taylor state geomagnetic field including polarity reversals on the Earth Simulator, *Science* 309 (2005) 459–461.
- [13] M. Kono, P.H. Roberts, Recent geodynamo simulations and observations of the geomagnetic field, *Rev. Geophys.* 40 (4) (2002) 1013, doi:10.1029/2000RG000102.
- [14] S. Stanley, J. Bloxham, Convective-region geometry as the cause of Uranus's and Neptune's unusual magnetic fields, *Nature* 428 (2004) 151–153.
- [15] J. Aubert, J. Wicht, Axial and equatorial dipolar dynamo action in rotating spherical shells, *Earth Planet. Sci. Lett.* 221 (2004) 409419.
- [16] M.H. Heimpel, J.M. Aurnou, F.M. Al-Shamali, N. Gomez Perez, A numerical study of dynamo action as a function of spherical shell geometry, *Earth Planet. Sci. Lett.* 236 (2005) 542–557, doi:10.1016/j.epsl.2005.04.032.
- [17] E. Dormy, J.P. Valet, V. Courtillot, Numerical models of the Geodynamo and observational constraints, *Geochem. Geophys. Geosyst.* 1 (2000), doi:10.1029/2000GC000062.
- [18] G.A. Glatzmaier, Geodynamo simulations — How realistic are they? *Annu. Rev. Earth Planet. Sci.* 30 (2002) 237–257.
- [19] G.A. Glatzmaier, P. Olson, Probing the Geodynamo, *Sci. Am.* 292 (2005) 50–57.
- [20] J. Aurnou, S. Aurnou, L. Zhu, P. Olson, Experiments on convection in Earth's core tangent cylinder, *Earth Planet. Sci. Lett.* 212 (2003) 119–134.
- [21] J. Aubert, Steady zonal flows in spherical shell dynamos, *J. Fluid Mech.* 542 (2005) 53–67.
- [22] U. Christensen, A. Tilgner, Power requirement of the geodynamo from ohmic losses in numerical and laboratory dynamos, *Nature* 439 (2004) 169–171.
- [23] S.V. Starchenko, C.A. Jones, Typical velocities and magnetic field strengths in planetary interiors, *Icarus* 157 (2002) 426–435.
- [24] P. Olson, U. Christensen, G.A. Glatzmaier, Numerical modeling of the geodynamo: mechanisms of field generation and equilibration, *J. Geophys. Res.* 104 (1999) 10,383–10,404.
- [25] F.H. Busse, E. Grote, R. Simitev, Convection in rotating spherical shells and its dynamo action, in: C.A. Jones, A.M. Soward, K. Zhang (Eds.), *Earth's Core and Lower Mantle*, Taylor and Francis, London, 2003, pp. 130–152.
- [26] U. Christensen, P. Olson, G.A. Glatzmaier, Numerical modeling of the geodynamo: a systematic parameter study, *Geophys. J. Int.* 138 (1999) 393–409.
- [27] C. Kutzner, U. Christensen, From stable dipolar to reversing numerical dynamos, *Phys. Earth Planet. Int.* 131 (2002) 29–45.
- [28] C. Kutzner, U. Christensen, Simulated geomagnetic reversals and preferred virtual geomagnetic pole paths, *Geophys. J. Int.* 157 (2004) 1105–1118.
- [29] P. Olson, U. Christensen, The time-averaged magnetic field in numerical dynamos with non-uniform boundary heat flow, *Geophys. J. Int.* 151 (2002) 809–823.
- [30] J. Wicht, P. Olson, A detailed study of the polarity reversal mechanism in a numerical dynamo model, *Geochem. Geophys. Geosyst.* 5 (2004), doi:10.1029/2003GC000602.
- [31] F. Takahashi, M. Matsushima, Dynamo action in a rotating spherical shell at high Rayleigh numbers, *Phys. Fluids* 17 (2005) 076601.
- [32] U.R. Christensen, J. Aubert, Scaling properties of convection-driven dynamos in rotating spherical shells and application to planetary magnetic fields, *Geophys. J. Int.* 166 (2006) 97–114.
- [33] B.A. Buffett, The thermal state of the Earth's core, *Science* 299 (2003) 1675–1676.
- [34] S. Labrosse, Thermal and magnetic evolution of the Earth's core, *Phys. Earth Planet. Inter.* 140 (2003) 127–143.
- [35] F. Nimmo, G.D. Price, J. Brodholt, D. Gubbins, The influence of potassium on core and geodynamo evolution, *Geophys. J. Int.* 156 (2004) 363–376.
- [36] J.A. Pirraglia, Meridional energy balance of Jupiter, *Icarus* 59 (1984) 169–176.
- [37] F. Nimmo, D.J. Stevenson, Why does Venus lack a magnetic field? *Geology* 30 (11) (2002) 987–990.
- [38] C.T. Russell, Scaling law test and two predictions of planetary magnetic moments, *Nature* 281 (1979) 552–553.
- [39] G. Schubert, V.S. Solomotov, P.J. Tackley, D.L. Turcotte, Mantle convection and the thermal evolution of Venus, in: S.W. Bougher, et al., (Eds.), *Venus II*, University of Arizona Press, Tucson, AZ, 1997, pp. 1245–1287.
- [40] G. Schubert, M.N. Ross, D.J. Stevenson, T. Spohn, Mercury's thermal history and the generation of its magnetic field, in: F. Vilas, et al., (Eds.), *Mercury*, University of Arizona Press, Tucson, AZ, 1988, pp. 429–460.
- [41] R.A. Secco, H.H. Schloessin, The electrical resistivity of solid and liquid Fe at pressures up to 7 GPa, *J. Geophys. Res.* 94 (1989) 5887–5894.
- [42] M.H. Acuna, J.E. Connerney, P. Wasilewski, et al., Magnetic field of Mars: summary of results from the aerobraking and mapping orbits, *J. Geophys. Res., Planets* 106 (2001) 23403–23417.
- [43] A.P. Boss, Formation of gas and ice giant planets, *Earth Planet. Sci. Lett.* 202 (2002) 513–523.
- [44] T. Guillot, Interiors of giant planets in side and outside the solar system, *Science* 286 (1999) 72–77.
- [45] W.J. Nellis, Metallization of fluid hydrogen at 140 GPa (1.4 Mbar): implications for Jupiter, *Planet. Space Sci.* 48 (2000) 671–766.
- [46] J.J. Fortney, W.B. Hubbard, Phase separation in giant planets: inhomogeneous evolution of Saturn, *Icarus* 164 (2003) 228–243.
- [47] M.K. Dougherty, N. Achilleos, N. Andre, et al., Cassini magnetometer observations during Saturn orbit insertion, *Science* 307 (2005) 1266–1270.
- [48] M. Podolak, W.B. Hubbard, D.J. Stevenson, in: J.T. Bergstrahl, E.D. Miner, M.S. Matthews (Eds.), *Uranus*, Univ. Arizona Press, Tucson, 1991.
- [49] W.B. Hubbard, M. Podolak, D.J. Stevenson, The interior of Neptune, Neptune and Triton, University of Arizona Space Science Series, 1995, pp. 109–138.
- [50] J.G. Williams, D.H. Boggs, C.F. Yoder, et al., Lunar rotational dissipation in solid body and molten core, *J. Geophys. Res., Planets* 106 (2001) 27933–27968.
- [51] M.G. Kivelson, K.K. Khurana, M. Volwerk, The permanent and inductive magnetic moments of Ganymede, *Icarus* 157 (2) (2002) 507.
- [52] B. Sreenivasan, C. Jones, The role of inertia in the evolution of spherical dynamos, *Geophys. J. Int.* 164 (2006) 467–476.
- [53] S. Stanley, J. Bloxham, W.E. Hutchinson, M.T. Zuber, Thin shell dynamos consistent with Mercury's weak observed magnetic field, *Earth Planet. Sci. Lett.* 234 (2005) 27–38.
- [54] F. Takahashi, M. Matsushima, Dipolar and non-dipolar dynamos in a thin shell geometry with implications for the magnetic field of Mercury, *Geophys. Res. Lett.* 33 (2006) L10202.
- [55] P.A. Gilman, Dynamically consistent nonlinear dynamos driven by convection in a rotating spherical shell: II. Dynamos with cycles and strong feedbacks, *Astrophys. J.* 53 (1983) 243–268.